

# Molecular Structure and Bonding of Copper Cluster Monocarbonyls $\text{Cu}_n\text{CO}$ ( $n = 1-9$ )

**Albert Poater and Miquel Duran**

*Institut de Química Computacional and Departament de Química, Universitat de Girona, E-17071 Girona, Catalonia, Spain*

**Pablo Jaque and Alejandro Toro-Labbé\***

*Laboratorio de Química Teórica Computacional (QTC), Facultad de Química, Pontificia Universidad Católica de Chile, Casilla 306, Correo 22, Santiago, Chile*

**Miquel Solà\***

*Institut de Química Computacional and Departament de Química, Universitat de Girona, E-17071 Girona, Catalonia, Spain*

*Received: August 19, 2005; In Final Form: December 2, 2005*

In this work we analyze CO binding on small neutral copper clusters,  $\text{Cu}_n$  ( $n = 1-9$ ). Molecular structures and reactivity descriptors of copper clusters are computed and discussed. The results show that the condensed Fukui functions and the frontier molecular orbital theory are useful tools to predict the selectivity of CO adsorption on these small clusters. To get further insight into the CO binding to copper clusters, an energy decomposition analysis of the CO binding energy is performed. The  $C_s$  symmetry of the formed  $\text{Cu}_n\text{CO}$  clusters ( $n = 1-8$ ) allows the separation between the orbital interaction terms corresponding to donation and back-donation. It is found that, energetically, the donation is twice as important as back-donation.

## 1. Introduction

Transition metal clusters are particularly interesting for their potential use in homogeneous and heterogeneous catalysis and novel optoelectronic materials.<sup>1-3</sup> The number of works devoted to the analysis of metal clusters has grown considerably over the past years as new experimental and theoretical techniques have been developed allowing detailed characterization of this type of systems. These small species are extremely sensitive to the number of atoms, and their properties can sometimes change dramatically with the addition or removal of one or a few atoms from the cluster. Most studies in this field have analyzed the dependences of different properties, such as ionization potentials, electron affinities, chemical reactivity, thermochemistry, and ion abundances upon the size of the clusters<sup>4</sup> and how these properties tend to the bulk values.<sup>5,6</sup>

In particular, copper clusters have been studied extensively both experimentally and theoretically.<sup>7-29</sup> From a theoretical point of view, density functional theory (DFT) calculations for small copper clusters ( $\text{Cu}_n$ , up to  $n = 5$ ) have been performed by Calaminici et al.<sup>21</sup> to predict their structures and electronic properties. Jackson has extended this investigation to the electronic properties of the smallest copper clusters,<sup>25</sup> concluding that the participation of the 3d and 4s orbitals of copper in the bonding states of the clusters is significant. Jaque and Toro-Labbé have analyzed the stability and reactivity pattern of the neutral clusters, showing that clusters with an even number of copper atoms and a closed-shell electronic structure are more stable than those with an odd number of copper atoms.<sup>29</sup> The static polarizabilities and polarizability anisotropies of copper clusters have been reported by Jackson and Calaminici and co-

workers.<sup>23</sup> On the other hand, Jug et al. have investigated the electronic and molecular structure of the most stable anionic, cationic, and neutral small copper clusters.<sup>26</sup> Finally, other studies have compared the properties of these small clusters with those of the copper surface.<sup>30,31</sup>

The interaction of metal clusters with small molecules has centered part of the interest of several works.<sup>32-35</sup> For  $\text{Cu}_n\text{CO}$  clusters, Cao et al.<sup>32</sup> have observed that the static mean polarizability increases monotonically as the size of the copper cluster carbonyl increases, while the mean polarizability per atom has a decreasing oscillating behavior. In that paper, the authors have also computed the CO binding energies and have discussed the selectivity of CO adsorption on copper clusters. Despite their important contribution, Cao and co-workers<sup>32</sup> did not analyze in their work the nature of the chemical bond in copper cluster monocarbonyls. In particular, the study of the relative importance of donation and back-donation in the binding of CO to  $\text{Cu}_n$  as a function of the size of the cluster remains to be done yet. Here, we report an accurate structural and electronic characterization of neutral copper clusters  $\text{Cu}_n$  ( $n = 1-9$ ) and of their monocarbonyls. The binding of CO to  $\text{Cu}_n$  is analyzed by means of an energy decomposition analysis that allows separating the contributions of donation and back-donation to the total CO binding energy. Previous works have shown the relevance of chemical electronic reactivity descriptors such as the chemical potential ( $\mu$ ), chemical hardness ( $\eta$ ), and electrophilicity index ( $\omega$ ), defined within the framework of DFT to understand the reactivity pattern of molecules and molecular aggregates.<sup>5,29-31,36-39</sup> In the present work, we discuss the use of the condensed Fukui functions to predict the selectivity of CO adsorption on copper clusters.

\* Corresponding authors. E-mail: miquel.sola@udg.es, atola@puc.cl.

## 2. Theoretical Background

**A. Reactivity Descriptors in the Framework of the Conceptual Density Functional Theory.** The Fukui function<sup>40</sup> is a reactivity index that connects the concepts of the Fukui frontier molecular orbitals with DFT. It was defined by Yang and Parr as the partial derivative of the electron density with respect to the total number of electrons at a constant external potential, or as the derivative of the chemical potential with respect to the external potential, keeping constant the total number of electrons of the system:

$$f(\vec{r}) = \left( \frac{\delta\mu}{\delta\nu(\vec{r})} \right)_N = \left( \frac{\partial\rho(\vec{r})}{\partial N} \right)_{\nu(\vec{r})} \quad (1)$$

The Fukui function describes the local changes in the electronic density of a system due to a perturbation in the total number of electrons. For a molecule or an atom, the right-hand derivative of eq 1 is not continuous with the number of electrons and is difficult to evaluate.<sup>41,42</sup> So, Parr and Yang<sup>40</sup> defined the Fukui functions  $f^+(\vec{r})$ ,  $f^-(\vec{r})$ , and  $f^0(\vec{r})$  corresponding to the reactivity index that describes the attack toward our system by a nucleophile, electrophile, or a radical species:

$$f^+(\vec{r}) = \left( \frac{\partial\rho(\vec{r})}{\partial N} \right)_{\nu(\vec{r})}^+ \quad (2)$$

$$f^-(\vec{r}) = \left( \frac{\partial\rho(\vec{r})}{\partial N} \right)_{\nu(\vec{r})}^- \quad (3)$$

$$f^0(\vec{r}) = \left( \frac{\partial\rho(\vec{r})}{\partial N} \right)_{\nu(\vec{r})}^0 \quad (4)$$

where the superindices +, -, and 0 refer to the right, left, and central derivatives, respectively. If we apply the same technique of the finite differences used in the chemical potential and the hardness to eqs 2–4 we obtain that the Fukui functions can be evaluated from the following density differences:<sup>43</sup>

$$f^+(\vec{r}) = \rho_{N+1}(\vec{r}) - \rho_N(\vec{r}) \quad (5)$$

$$f^-(\vec{r}) = \rho_N(\vec{r}) - \rho_{N-1}(\vec{r}) \quad (6)$$

$$f^0(\vec{r}) = \frac{1}{2}[\rho_{N+1}(\vec{r}) - \rho_{N-1}(\vec{r})] \quad (7)$$

If eqs 5–7 are integrated within specific regions of the molecular topology, we obtain the corresponding condensed Fukui functions:

$$f_x^+ = q_x(N+1) - q_x(N)$$

$$f_x^- = q_x(N) - q_x(N-1)$$

$$f_x^0 = \frac{1}{2}[q_x(N+1) - q_x(N-1)] \quad (8)$$

where the parameters  $q_x$  are the charges of the atom X calculated in the systems with  $N$ ,  $N-1$ , and  $N+1$  electrons at the optimized geometry of the molecule with  $N$  electrons. Over the past years, the condensed Fukui functions have been used to explain the regioselectivity in chemical reactions, especially in cycloaddition reactions.<sup>44</sup>

**B. Energy Decomposition Analysis and Mayer Bond Orders.** By the energy decomposition analysis (EDA),<sup>45</sup> the total binding energy (BE) between two fragments in a molecule

is divided into deformation energy and interaction energy ( $BE = \Delta E_{\text{def}} + \Delta E_{\text{int}}$ ). The deformation energy ( $\Delta E_{\text{def}}$ ) is the energy needed to modify the geometry of the ground-state free fragments to attain the geometry they have in the intermediate. The interaction energy ( $\Delta E_{\text{int}}$ ) is the energy released when the two free deformed fragments are brought to the position that they have in the intermediate, and it has been, in turn, splitted into electrostatic, Pauli repulsion, and orbital interaction terms ( $\Delta E_{\text{int}} = \Delta E_{\text{elstat}} + \Delta E_{\text{Pauli}} + \Delta E_{\text{oi}}$ ). The term  $\Delta E_{\text{elstat}}$  corresponds to the classical electrostatic interaction between the unperturbed charge distributions of the prepared fragments and it is usually attractive.<sup>46</sup> The Pauli repulsion term,  $\Delta E_{\text{Pauli}}$ , comprises the destabilizing interactions between occupied orbitals and is responsible for the steric repulsion. This repulsion is caused by the fact that two electrons with the same spin cannot occupy the same region in space. The term comprises the four-electron destabilizing interactions between occupied orbitals. The orbital interaction term,  $\Delta E_{\text{oi}}$ , accounts for charge transfer (interaction between occupied orbitals on one moiety with unoccupied orbitals of the other, including the HOMO–LUMO interactions) and polarization (empty occupied orbital mixing on one fragment due to the presence of another fragment). The latter term can be further partitioned into contributions of the orbitals which belong to different irreducible representations of the point group of the interacting system. Due to the fact that orbital interactions ( $\Delta E_{\text{oi}}$ ) can be associated to the covalent bond contributions and the electrostatic term ( $\Delta E_{\text{elstat}}$ ) to the ionic ones, the  $\Delta E_{\text{elstat}}/(\Delta E_{\text{elstat}} + \Delta E_{\text{oi}})$  term provides a measure of the ratio of the ionic character of the studied bonds.

Finally, we have calculated Mayer bond orders through the expression<sup>47</sup>

$$B_{AB} = 2 \sum_{\mu \in A} \sum_{\nu \in B} [(P^{\alpha}S)_{\mu\nu}(P^{\alpha}S)_{\nu\mu} + (P^{\beta}S)_{\mu\nu}(P^{\beta}S)_{\nu\mu}] \quad (9)$$

where S is the atomic orbital overlap matrix and  $P^{\alpha}$  and  $P^{\beta}$  are the density matrices for the  $\alpha$  and  $\beta$  electrons, respectively.

## 3. Computational Methods

The reported calculations were carried out by using the 2002.03 release of Amsterdam density functional (ADF) package<sup>49</sup> developed by Baerends et al.<sup>50–52</sup> The numerical integration scheme employed was that of te Velde and Baerends.<sup>53</sup> Both geometry optimizations and energy evaluations were performed using a generalized gradient approximation (GGA) that includes the GGA exchange correction of Becke<sup>54</sup> and the GGA nonlocal correlation of Perdew and Wang,<sup>55</sup> that is, the so-called BPW91 functional. The optimization process was based on the gradients scheme developed by Ziegler et al.<sup>56</sup> The vibrational harmonic frequencies were calculated by the force constants obtained by the numerical differentiation of the energy gradients.<sup>57</sup> The kinetic relativistic effects are not important for an accurate calculation of copper clusters and they were ignored in our calculations.<sup>58</sup> All calculations were performed using an uncontracted triple- $\zeta$  basis set augmented with two polarization functions for describing the 3s, 3p, 3d, 4s, and 4p orbitals of copper and the 2s and 2p of carbon and oxygen.<sup>59,60</sup> Electrons in lower shells were treated within the frozen core approximation.<sup>50</sup> A set of auxiliary s, p, d, f, and g functions, centered in all nuclei, was introduced in order to fit the molecular density and Coulomb potential accurately in each SCF cycle.<sup>61</sup> Molecular orbitals were depicted using the Molekel program.<sup>62</sup>

Depending on the number of copper atoms of each cluster, clusters have an even or odd number of electrons. For this

**TABLE 1: Theoretical and Experimental Results for Some of the Structural and Electronic Properties of Cu<sub>2</sub>**

property	LSDA <sup>a</sup>	PW86/VWN <sup>b</sup>	PBE <sup>c</sup>	BLYP <sup>d</sup>	B3LYP <sup>e</sup>	B3PW91 <sup>c</sup>	BPW91	exptl
$r_0$ (Å)	2.18	2.21	2.27	2.257	2.18	2.254	2.227	2.22 <sup>f</sup>
$\nu$ (cm <sup>-1</sup> )	292	269	236	263	256	260	267	265 <sup>f</sup>
BE (eV) <sup>g</sup>	2.72	2.22 (2.08)	2.21	2.1	2.02	1.93	1.95 (1.91)	2.08 <sup>h</sup>
IP (eV)	8.61	8.73	8.36	—	—	7.80	8.23	7.9042 <sup>i</sup>
EA (eV)	0.97	0.96	0.93	—	—	0.59	0.83	0.836 <sup>j</sup>

<sup>a</sup> From ref 25. <sup>b</sup> From ref 26. <sup>c</sup> From ref 29. <sup>d</sup> From ref 63. <sup>e</sup> From ref 32. <sup>f</sup> From ref 27. <sup>g</sup> In parentheses there are the BE values corrected by BSSE and ZPE. <sup>h</sup> From ref 28. <sup>i</sup> From ref 17. <sup>j</sup> From ref 15.

reason, optimizations were done checking different multiplicities to characterize the ground-states, either neutral closed-shell singlet and triplet multiplicities for systems with even number of electrons or open-shell doublet and quadruplet multiplicities for clusters with odd number of electrons. Calculations of open-shell species have been performed within the unrestricted methodology, while the closed-shell singlet molecules have been calculated using the restricted formalism.

#### 4. Results and Discussion

This section is organized as follows. First, we validate the methodology employed by computing a series of chemical properties for the Cu<sub>2</sub> cluster, the simplest of the systems studied. Second, we discuss shortly the structures and the possible reactivity toward the CO molecule. Finally, we analyze the molecular structures and binding energies of CO in the copper cluster carbonyls and we examine the nature of the Cu–CO chemical bond.

**A. The Cu<sub>2</sub> Cluster: Validation of the Methodology.** We start this section by comparing our results for the smallest Cu<sub>2</sub> cluster with previous experimental and theoretical results.<sup>25–27,29</sup> Table 1 lists the Cu–Cu bond length ( $r_0$ ), the harmonic frequency, the binding energy (BE), the ionization potential (IP), the electron affinity (EA), and the hardness ( $\eta$ ) of the Cu<sub>2</sub> system obtained with the present BPW91/TZ2P method. For comparison purposes, Table 1 also contains values from other theoretical and experimental studies. In general, all GGA and hybrid functionals yield results close to the experimental values. It is found that the BPW91/TZ2P performs slightly better with respect to the rest of methodologies analyzed in the calculation of the bond length, frequency, and electron affinity. These results provide confidence on the reliability of the chosen method to reproduce the geometry and the electronic structure of copper clusters. Our BE for Cu<sub>2</sub> is close to that obtained with DFT hybrid methodologies and somewhat inferior to those given by the BLYP<sup>63</sup> and PW86/VWN<sup>26</sup> methods. Our BPW91 value of the BE for Cu<sub>2</sub> becomes slightly worse after the inclusion of the zero-point energy (ZPE) and the basis set superposition error (BSSE) corrections. Although the PW86/VWN method provides a better estimation of the Cu–Cu BE,<sup>26</sup> the rest of the calculated parameters are closer to the experimental results when using BPW91 for energy and geometry optimization calculations. For this reason and because the size of the systems treated in the present work prevents the use of higher levels of theory than DFT, we have decided to carry out our study at the BPW91 level.

**B. Bare Copper Clusters Cu<sub>n</sub> ( $n = 2–9$ ).** The optimized structures of the ground state of the studied neutral copper clusters are depicted in Figure 1. If the number of copper atoms is even, the ground state is singlet, and doublet otherwise. In the particular case of the Cu<sub>2</sub> cluster, the triplet excited state is 38.8 kcal·mol<sup>-1</sup> less stable than the singlet ground state. From Cu<sub>3</sub> to Cu<sub>6</sub> the most stable clusters are planar, and the rest are tridimensional (3D). These nine structures apart from being

energy minima represent the most stable structure for each  $n$ . Other structures of Cu<sub>5</sub>\* and Cu<sub>6</sub>\* are also depicted in Figure 1. These are not the most stable structures for the bare copper clusters, but they become the most stable in the corresponding copper cluster carbonyls. The Supporting Information contains the results from other less stable structures of these neutral Cu<sub>n</sub> ( $n = 2–9$ ) clusters. The Supporting Information also includes the frequencies of the copper clusters, which are similar to those reported in previous works.<sup>26</sup>

It is worth mentioning that the linear Cu<sub>3</sub> copper cluster is 5.1 kcal·mol<sup>-1</sup> less stable than the triangular conformer. As to Cu<sub>5</sub>, the C<sub>2v</sub> planar isomer of trapezoidal structure is 6.0 and 7.2 kcal·mol<sup>-1</sup> more stable than the tridimensional clusters of C<sub>2v</sub> and D<sub>3h</sub> symmetry, respectively. The interconversion between the C<sub>2v</sub> trapezoidal Cu<sub>5</sub> cluster and the C<sub>2v</sub> distorted trigonal bipyramid Cu<sub>5</sub>\* cluster takes place through a transition state with a very low energy barrier, according to the calculations by Cao and co-workers.<sup>32</sup> For Cu<sub>6</sub>, the planar D<sub>3h</sub> structure is the global minimum, in agreement with previous Car–Parinello studies.<sup>64</sup> At the LDA level, three possible geometries of Cu<sub>6</sub> (planar D<sub>3h</sub> and tridimensional C<sub>2v</sub> and C<sub>5v</sub>) lie close in energy.<sup>26</sup> Our BPW91/TZ2P calculations indicate that the planar D<sub>3h</sub> isomer is 2.3 kcal·mol<sup>-1</sup> and 5.9 kcal·mol<sup>-1</sup> more stable than the C<sub>5v</sub> and C<sub>2v</sub> species, respectively. We have found in agreement with all studies made before,<sup>26,29,32</sup> that the most stable heptamer of Cu has a 3D structure of D<sub>5h</sub> symmetry. Planar structures of Cu<sub>7</sub> were found to lie higher in energy. Other 3D structures were also checked, but they were found to be destabilized by at least 5 kcal·mol<sup>-1</sup>.

The geometry optimizations of the Cu<sub>8</sub> and Cu<sub>9</sub> clusters were started from the most stable Cu<sub>7</sub> structure. The global minima for the Cu<sub>8</sub> and Cu<sub>9</sub> clusters adopt C<sub>2v</sub> symmetry. The Cu<sub>8</sub> cluster with C<sub>s</sub> symmetry, which was wrongly assigned as the most stable by Cao and co-workers,<sup>32</sup> is 3.2 kcal·mol<sup>-1</sup> less stable than the C<sub>2v</sub> one at the BPW91/TZ2P level and 3.7 kcal·mol<sup>-1</sup> with the B3LYP/DZP method used by Cao et al.<sup>32</sup> In addition, the Cu<sub>8</sub> cluster with T<sub>d</sub> symmetry appears only 0.1 kcal·mol<sup>-1</sup> higher in energy with respect to the cluster with C<sub>2v</sub> symmetry. Two other Cu<sub>9</sub> structures with C<sub>2v</sub> and C<sub>3v</sub> symmetry are 1.3 and 5.5 kcal·mol<sup>-1</sup> less stable than the C<sub>2v</sub> structure depicted in Figure 1, respectively.

**C. Reactivity Predictors.** We have calculated the condensed Fukui functions to predict the selectivity of CO adsorption on copper clusters. With CO characterized as a nucleophilic species, one could expect that the  $f^+$  would be the best Fukui function to predict the CO preferred binding sites. The metal–CO bond is usually<sup>65</sup> discussed in terms of the familiar Dewar–Chatt–Duncanson (DCD) model,<sup>66</sup> considering that the two synergistic main bonding interactions are  $\sigma$  donation from the carbon atom lone pair orbital of the CO into the empty d( $\sigma$ ) orbital of the metal, and  $\pi$  back-donation from an occupied d( $\pi$ ) metal atomic orbital to the empty  $\pi^*$  orbital of CO. Then, CO acts in copper cluster carbonyls not only as a nucleophile transferring electronic charge to the copper cluster, but also as an electrophile by

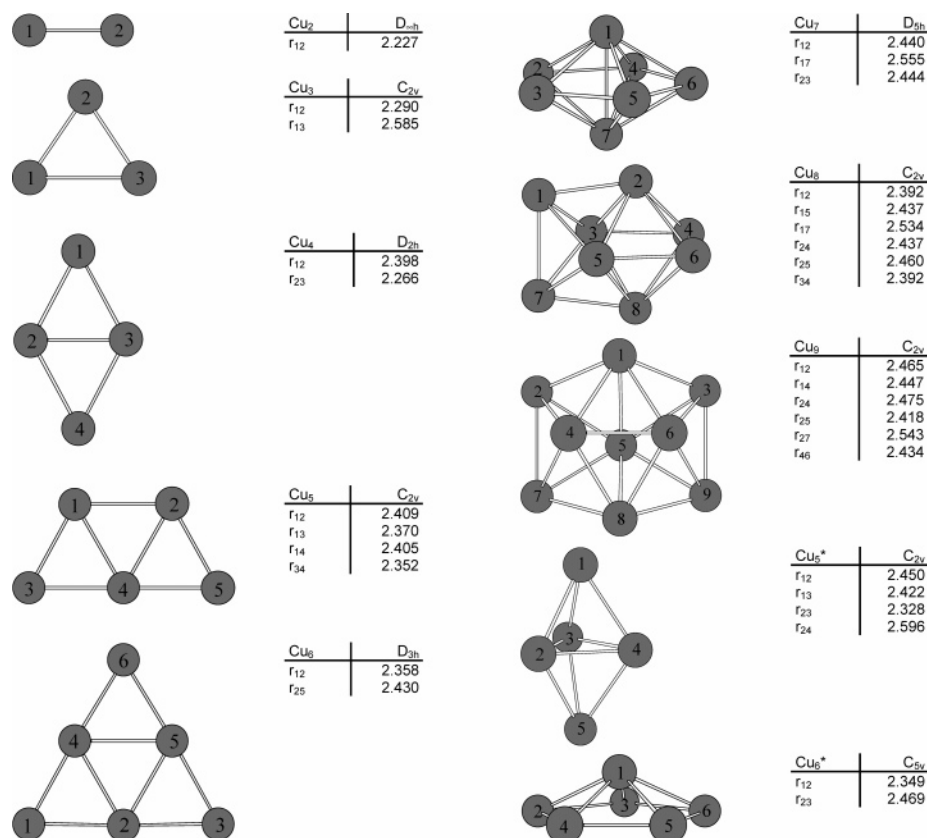


Figure 1. Structures of the most stable neutral copper clusters Cu<sub>n</sub> (n = 2–9) (distances in Å).

TABLE 2: Condensed Fukui Functions (electrons) for Copper Clusters Cu<sub>n</sub> (for atom numbering see Figure 1)

n	atom	f <sup>-</sup>		f <sup>+</sup>		f <sup>0</sup>	
		Mulliken	Hirshfeld	Mulliken	Hirshfeld	Mulliken	Hirshfeld
2	Cu1,2	0.500	0.500	0.500	0.500	0.500	0.500
3	Cu2	0.226	0.225	0.183	0.221	0.204	0.230
	Cu1,3	0.387	0.388	0.408	0.390	0.398	0.389
4	Cu1,4	0.314	0.336	0.207	0.214	0.260	0.275
	Cu2,3	0.186	0.164	0.293	0.286	0.240	0.225
5	Cu3,5	0.175	0.218	0.307	0.242	0.241	0.230
	Cu4	0.156	0.146	0.082	0.119	0.119	0.132
	Cu1,2	0.208	0.209	0.191	0.199	0.199	0.204
6	Cu1,3,6	0.202	0.209	0.347	0.259	0.274	0.234
	Cu2,4,5	0.131	0.124	-0.013	0.074	0.059	0.099
7	Cu2,3,4,5,6	0.133	0.129	0.128	0.131	0.131	0.130
	Cu1,7	0.167	0.177	0.179	0.172	0.173	0.174
8	Cu1,7	0.141	0.149	0.227	0.180	0.184	0.164
	Cu3,5	0.115	0.095	0.023	0.070	0.069	0.083
	Cu4,6	0.126	0.122	0.227	0.180	0.177	0.151
	Cu2,8	0.118	0.134	0.023	0.070	0.070	0.102
9	Cu5	0.033	0.032	0.014	0.029	0.024	0.031
	Cu4,6	0.074	0.070	0.066	0.067	0.070	0.068
	Cu2,3,7,9	0.160	0.162	0.177	0.166	0.169	0.164
5*	Cu1,8	0.089	0.089	0.073	0.086	0.081	0.088
	Cu3	0.151	0.138	0.430	0.406	0.290	0.272
	Cu2,4	0.247	0.255	0.119	0.118	0.183	0.186
6*	Cu1,5	0.177	0.176	0.167	0.180	0.172	0.178
	Cu2,3,4,5,6	0.167	0.163	0.174	0.166	0.170	0.164
	Cu1	0.103	0.079	0.131	0.172	0.117	0.126

receiving electrons from the metal cluster. Thus, given the complexity of CO bonding, the  $f^-$  and  $f^0$  have been also studied.<sup>67</sup>

The present condensed Fukui function analysis has been carried out using the Mulliken, Hirshfeld, and Voronoi charges. Although there is a general agreement that the Hirshfeld are more accurate than the Mulliken charges,<sup>67a,68</sup> we have included in Table 2 condensed Fukui functions obtained by eq 8 derived from both the Mulliken and Hirshfeld charges to allow for

comparisons. The condensed Fukui functions from Voronoi charges are listed in the Supporting Information because the results from Voronoi charges are completely equivalent to those obtained from the Hirshfeld charges.

The two positions of Cu<sub>2</sub> have obviously the same probability to be attacked and, therefore, the condensed Fukui functions do not provide new information in this case. For Cu<sub>3</sub>, the two atoms connected through the longest bond distance are the most reactive in front of a chemical attack. As to Cu<sub>4</sub>, condensed

Fukui functions point out the copper atoms in the long diagonal of the rhombus as the most easily attacked, except for the  $f^+$  function. The external positions of the large basis of the trapezium in  $\text{Cu}_5$  are the most reactive sites for CO binding except for the Mulliken  $f^-$  values, which indicate that the small basis copper atoms are the most reactive. For  $\text{Cu}_6$ , the most favored sites are the three vertices of the external triangle, while for  $\text{Cu}_7$ , the two copper atoms located in the tips of the pentagonal bipyramid have the highest Fukui function values. In  $\text{Cu}_8$ , the atoms numbered 1 and 7 in Figure 1 are the most reactive in front of any chemical attack.  $\text{Cu}_9$  have four positions partially more favored than the rest, which are those closer to the copper atom number 5 forming a rectangle. For  $\text{Cu}_5^*$ , copper number 3 presents the higher values, except for  $f^-$ , which yields the other two positions of the basis of the trigonal pyramid as the most reactive. In  $\text{Cu}_6^*$ , the basis positions are the most favored sites, except for the Hirshfeld  $f^+$  value. It is worth noting that, with few exceptions, the three types of the Fukui condensed functions obtained using three different definitions of atomic charge yield similar predictions as to the selectivity of CO adsorption on copper clusters. In addition, we have verified that the trends in reactivity predicted by the hard and soft acids and bases (HSAB) principle<sup>69</sup> using the local softness values<sup>70</sup> given in Table S2 of the Supporting Information are the same as those predicted by the condensed Fukui functions with the exception of  $\text{Cu}_3$ , for which atom 2 is the most reactive according to the HSAB principle prediction.

Another approach for predicting the most favorable site for the CO interaction with the copper cluster is the frontier molecular orbital (FMO) theory. For open-shell systems, because of the presence of an unpaired electron, we have taken as the HOMO the highest  $\alpha$  occupied orbital and as the LUMO the lowest  $\beta$  unoccupied orbital.

The representation of the frontier molecular orbitals of copper clusters ( $n = 1-9$ ) allows us to make a prediction of the more favorable adsorption sites. Due to the dominant donor character of the monoxide molecule in this interaction (vide infra), the most important orbitals to be considered are the LUMO of the cluster and the HOMO of the CO molecule. At the same time, in the DCD scheme, there is back-donation of the copper cluster toward CO. Therefore, it is necessary to take into account also, as a secondary important interaction, that between the HOMO of the cluster and the LUMO of CO. The representation of the HOMO and LUMO orbitals of the CO and the  $\text{Cu}_n$  clusters is displayed in Figure 2.

From the LUMO orbitals in Figure 2 it is possible to predict the copper atoms in a given cluster that, in theory, will interact better with CO, which are those having larger contributions to the LUMO orbital. Following this criterion, the central copper would be the most reactive atom of  $\text{Cu}_3$ , but the significant component of the LUMO corresponding to the external atoms indicates that these atoms may also interact favorably with CO. The copper atoms of the short diagonal of the rhombus of  $\text{Cu}_4$  and the atoms of the short basis of the trapezium in  $\text{Cu}_5$  are expected to be the most reactive, while the three vertices of the external triangle in  $\text{Cu}_6$ , the tips of the pentagonal bipyramid in  $\text{Cu}_7$ , two the most external positions of  $\text{Cu}_8$ , and one of the four extreme positions in  $\text{Cu}_9$  are predicted to be the most suitable for the CO nucleophilic attack according to the shape of the LUMO orbitals. As to the less stable clusters, any position of the basis and the vertex of the pentagonal pyramid are the most reactive sites in  $\text{Cu}_5^*$  and  $\text{Cu}_6^*$ , respectively.

It is worth noting that a comparison between the predicted results from the condensed Fukui functions and the frontier

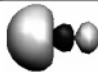





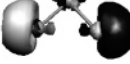







orbitals shows that, although the theoretical background is different for both approaches, the results are nearly the same, especially when the cluster presents an even number of copper atoms.

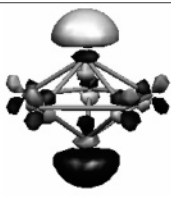
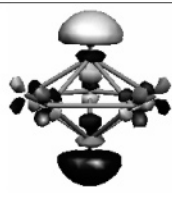
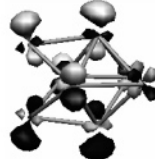
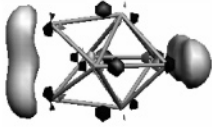
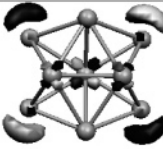
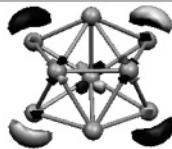




**D. Copper Cluster Carbonyls  $\text{Cu}_n\text{CO}$  ( $n = 1-9$ ).** *1. Structures and Stabilities.* The CO molecules can be adsorbed on the copper surfaces with terminal or bridge coordination. Although we focus our study only on the former, we have checked that the bond bridge coordination is either unattainable or less stable in all cases. Figure 3 depicts the most stable geometrical structures of copper cluster carbonyls for each  $n$  ( $n = 1-9$ ). In the clusters with five and six copper atoms, the CO binding results in important geometrical changes of the initially most stable planar copper cluster structure. Thus, the  $\text{Cu}_5\text{CO}$  cluster adopts a trigonal bipyramidal (tbp) structure with the CO attached to a copper atom of the triangular base while the  $\text{Cu}_6\text{CO}$  species takes a pentagonal pyramidal arrangement with the CO bonded to the tip of the pyramid.

$\text{Cu}_1\text{CO}$  does not present a linear structure because the overlap between the HOMO orbital of the copper and the  $2\pi^*$  LUMO orbital of CO favors a nonlinear arrangement. The BPW91/TZ2P optimized geometry of  $\text{Cu}_2\text{CO}$  is linear. This is in contradiction with the angular structure reported by Cao and co-workers.<sup>32</sup> All attempts to optimize an angular structure with the BPW91/TZ2P method reverted to the present linear one. Repeating the calculations made by Cao et al.,<sup>32</sup> with the same functional and basis set used by these authors (B3LYP/DZP), we found that the nonlinear structure is only  $0.08 \text{ kcal}\cdot\text{mol}^{-1}$  more stable than the linear arrangement. This means that the difference between linear and angular structures for  $\text{Cu}_2\text{CO}$  is very small, and that little changes in the method and basis set used may lead to different optimized structures. Unexpectedly, after the interaction with CO, the  $\text{Cu}_3$  cluster adopts an almost equilateral triangle geometry with the shortening of the  $\text{Cu}1-\text{Cu}3$  bond that before the introduction of CO was the longest. We also found a stable linear structure for  $\text{Cu}_3\text{CO}$ , which is  $16.8 \text{ kcal}\cdot\text{mol}^{-1}$  higher in energy as compared to the triangular arrangement. The CO can interact with  $\text{Cu}_4$  in two different ways, either through the main or the short diagonals, the latter being the most favorable.

While the bare  $\text{Cu}_5$  cluster presents a planar trapezoidal structure, this fragment in the most stable  $\text{Cu}_5\text{CO}$  species adopts tbp geometry. For the trapezoidal structure, the two copper atoms of the short basis are favored. As a result of the CO interaction this basis becomes markedly elongated, thus anticipating future likely distortions of this planar  $\text{Cu}_5\text{CO}$  structure that would lead to the  $D_{3h}$  tbp geometry. A similar phenomenon is found in the copper cluster carbonyl with six copper atoms. The initial planar structure of the  $\text{Cu}_6$  cluster changes in the  $\text{Cu}_6\text{CO}$  complex to a pentagonal pyramidal geometry of  $C_{5v}$  symmetry. The most favorable interaction takes place at the tip of the pentagonal pyramid. The CO interaction at one of the three vertices of the planar triangular  $D_{3h}$   $\text{Cu}_6$  cluster leads to a  $\text{Cu}_6\text{CO}$  species with  $C_s$  symmetry. The  $\text{Cu}_5$  and  $\text{Cu}_6$  clusters adopt a 3D structure after the interaction with a CO molecule confirming the predictions by Jug, Zimmermann, and Köster<sup>71</sup> made from the shape of the frontier molecular orbitals.

Unlike in  $\text{Cu}_6$ , the CO binding in  $\text{Cu}_7$  in the positions of the pentagonal bipyramid basis to yield a  $\text{Cu}_7\text{CO}$  species of  $C_s$  symmetry is  $4.5 \text{ kcal}\cdot\text{mol}^{-1}$  favored over the interaction with the tips that results in a  $C_{2v}$   $\text{Cu}_7\text{CO}$  cluster, in contradiction with the results reported by Cao et al.<sup>32</sup> It is worth noting that at the level of theory used by Cao and co-workers<sup>32</sup> (B3LYP/DZP) the  $C_{2v}$   $\text{Cu}_7\text{CO}$  cluster is more stable than the  $C_s$   $\text{Cu}_7\text{CO}$

	HOMO	LUMO
CO		
	-9.03	-1.99
Cu <sub>1</sub>		
	-5.06	-3.69
Cu <sub>2</sub>		
	-4.72	-2.86
Cu <sub>3</sub>		
	-4.90	-3.05
Cu <sub>4</sub>		
	-4.35	-3.32
Cu <sub>5</sub>		
	-4.76	-3.64
Cu <sub>6</sub>		
	-4.71	-2.73

Cu <sub>7</sub>		
	-4.72	-3.54
Cu <sub>8</sub>		
	-4.50	-2.95
Cu <sub>9</sub>		
	-4.40	-3.22
Cu <sub>5</sub> *		
	-4.38	-3.46
Cu <sub>6</sub> *		
	-4.58	-2.89

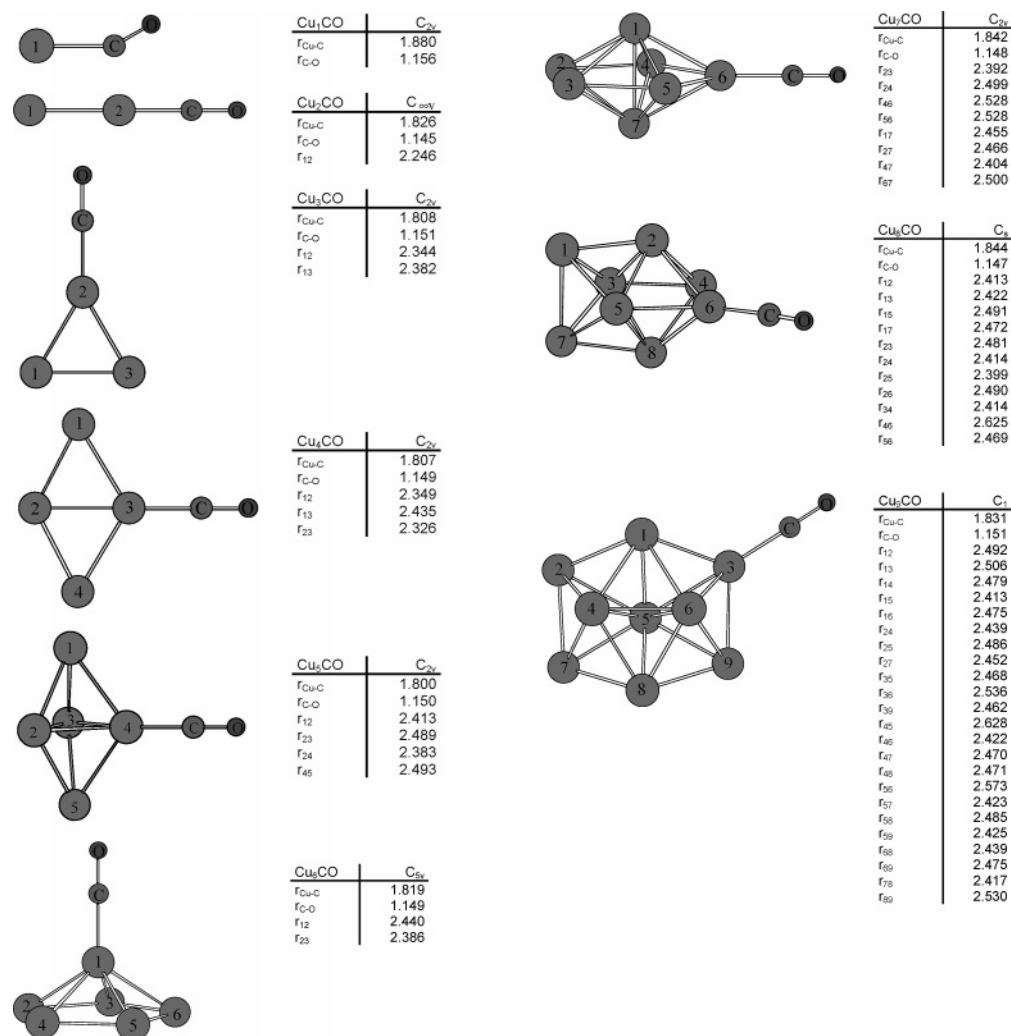
**Figure 2.** Representation of the HOMO and LUMO orbitals of CO and the copper clusters Cu<sub>*n*</sub>. The different gray tones of the orbitals represent the negative and the positive regions. Isosurface values are 0.05 and  $-0.05$  au. Below each orbital there is its corresponding energy in eV.

complex by  $2.2 \text{ kcal}\cdot\text{mol}^{-1}$  and by  $4.5 \text{ kcal}\cdot\text{mol}^{-1}$  when using B3LYP/6-31G\*. Thus, the trend in the relative stability of the C<sub>s</sub> and C<sub>2v</sub> Cu<sub>7</sub>CO clusters changes significantly depending on the method and basis set used, showing that the two structures have similar stabilities. In Cu<sub>8</sub> the most favorable copper atoms to be attacked are those numbered 1 and 7 in Figure 1. In Cu<sub>9</sub>, the attack occurs to any of the copper atoms numbered 2, 3, 7, and 9. The most favorable site for CO binding in Cu<sub>9</sub> found by Cao et al.<sup>32</sup> is less stable than our predicted position by about  $0.1 \text{ kcal}\cdot\text{mol}^{-1}$  and  $0.7 \text{ kcal}\cdot\text{mol}^{-1}$  at the BPW91/TZ2P and B3LYP/6-31G\* levels of theory, respectively.<sup>32</sup> These two structures are found very close in energy. Indeed, the relative stability of the two structures changes if we perform the calculations using the same method and basis set of double- $\xi$  quality containing pseudopotentials (B3LYP/DZP) employed by Cao et al.<sup>32</sup>

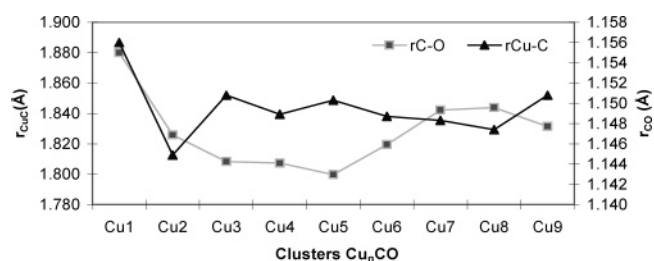
In general, the structure of the most stable copper cluster carbonyl for each value of *n* presents the strongest and shortest Cu–C bond and the weakest and longest C–O bond. This is in line with the DCD bonding scheme for the CO interaction with the copper clusters. In this bonding scheme, donation and back-donation act synergistically. Thus, a larger back-donation to the

$\pi^*$  unoccupied orbital of CO favors the  $\sigma$  donation of CO to the copper cluster, which in turn promotes the back-donation. As a result, a shorter and stronger Cu–C bond and a longer and weaker C–O bond are normally found as observed in Figure 4. The only exception to this general rule is Cu<sub>1</sub>CO, which follows a different behavior as compared to the rest of the clusters.<sup>29</sup> Cu–C and C–O frequencies for copper cluster monocarbonyls are listed in the Supporting Information.

Coming back to the results of the condensed Fukui functions, it is observed that most of the predictions done a priori have been accomplished. This is particularly true for the  $f^+$  function, which only fails for the prediction of the selectivity in Cu<sub>7</sub>. However, the difference between the  $f^+$  condensed Fukui functions for the 1 (7) and 2 (3–6) copper atoms is not large enough to totally discard the interaction through the 2–6 copper atoms, especially if one takes into account that the local reactivity may change by the external field generated by the approaching CO molecule. The  $f^-$  and  $f^0$  are unsuccessful to predict the correct reactive site of the Cu<sub>4</sub>, Cu<sub>6</sub>\*, and Cu<sub>7</sub> clusters. Thus, the  $f^+$  function is the most suitable for predicting the selectivity of the CO adsorption on copper clusters.



**Figure 3.** Geometries of the  $\text{Cu}_n\text{CO}$  copper cluster carbonyls ( $n = 1-9$ ) (distances in Å).



**Figure 4.** Evolution of the Cu-C and C-O distances (Å) in copper cluster carbonyls.

Predictions from the shape of the LUMO orbitals of the cluster are also satisfactory except for the  $\text{Cu}_7$  cluster.

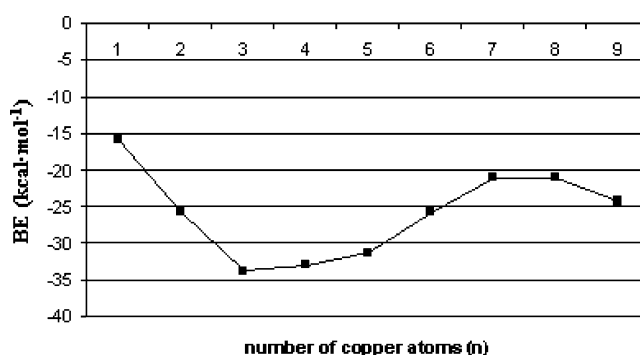
## 2. Binding Energies and the Nature of the Chemical Bond.

The BE of the CO molecules adsorbed on the copper clusters is calculated as

$$\text{BE} = E_{\text{Cu}_n\text{CO}}^{\text{multiplicity}} - (E_{\text{CO}}^{\text{free}} - E_{\text{Cu}_n}^{\text{free}}) \quad (10)$$

where the multiplicity can be either singlet in even-numbered copper clusters or doublet in odd-numbered ones.

The plot of the BE with respect to the size of the cluster is given in Figure 5. The BPW91/TZ2P BEs listed in Table 3 are clearly larger in absolute value than those reported by Cao et al.<sup>32</sup> Despite the numerical differences between our BEs and those reported by Cao and co-workers,<sup>32</sup> the trends are exactly the same, except for the fact that the open-shell  $\text{Cu}_5\text{CO}$  cluster



**Figure 5.** Plot of the CO binding energy (BE, kcal·mol<sup>-1</sup>) with respect to the number of copper atoms in the copper cluster carbonyls.

has the largest, in absolute value, BE at the BPW91/TZ2P level, while with the B3LYP/DZP method the strongest Cu-C bond corresponds to the  $\text{Cu}_5\text{CO}$  cluster.

To obtain a deeper insight into the nature of the Cu-CO bond in copper cluster carbonyls, an energy decomposition analysis (EDA) has been carried out. In this analysis, the total BE is divided into preparation energy and interaction energy ( $\text{BE} = \Delta E_{\text{prep}} + \Delta E_{\text{int}}$ ) of the copper cluster with the CO molecule. The preparation energy term ( $\Delta E_{\text{prep}}$ ) is the sum of the deformation energy ( $\Delta E_{\text{def}}$ ) and the excitation energy ( $\Delta E_{\text{excit}}$ ). The deformation energy is the energy needed to modify the geometry of the ground-state free fragments to attain the geometry that they have after the insertion of a CO molecule

**TABLE 3: Values of the Energy Decomposition Analysis of Cu–C Bond (in kcal·mol<sup>-1</sup>)**

clusters	$\Delta E_{\text{defCO}}$	$\Delta E_{\text{defCu}_n}$	$\Delta E_{\text{def}}$	$\Delta E_{\text{excit}}$	$\Delta E_{\text{prep}}$	$\Delta E_{\text{Pauli}}$	$\Delta E_{\text{elstat}}$	$\Delta E_{\text{oi}}$	$\Delta E_{\text{int}}$	BE <sup>a</sup>	% $\Delta E_{\text{elstat}}$
Cu <sub>1</sub> CO	0.5	0.0	0.5	6.6	7.1	165.7	-90.0	-98.8	-23.0	-15.9 (-14.4)	47.69
Cu <sub>2</sub> CO	0.1	0.0	0.1	0.0	0.1	130.6	-98.1	-58.3	-25.8	-25.7 (-23.0)	62.73
Cu <sub>3</sub> CO	0.3	1.0	1.3	5.5	6.8	231.2	-131.7	-140.1	-40.6	-33.8 (-30.4)	48.45
Cu <sub>4</sub> CO	0.2	0.5	0.7	0.0	0.7	132.1	-101.1	-64.7	-33.8	-33.0 (-29.2)	60.98
Cu <sub>5</sub> CO	0.3	6.6	6.9	5.6	12.5	212.8	-127.2	-129.4	-43.7	-31.2 (-26.8)	49.58
Cu <sub>6</sub> CO	0.3	4.9	5.2	0.0	5.2	133.3	-100.3	-64.0	-31.0	-25.8 (-20.9)	61.03
Cu <sub>7</sub> CO	0.2	1.1	1.3	2.5	3.8	140.4	-101.1	-64.2	-24.9	-21.0 (-16.4)	61.17
Cu <sub>8</sub> CO	0.2	1.0	1.2	0.0	1.2	139.0	-100.0	-61.2	-22.3	-21.1 (-16.1)	62.03
Cu <sub>9</sub> CO	0.3	1.1	1.4	2.2	3.6	160.6	-108.3	-80.3	-27.9	-24.3 (-18.6)	57.42

<sup>a</sup> In parentheses, the BE values corrected by BSSE and ZPE.

and has two components, the deformation of CO ( $\Delta E_{\text{defCO}}$ ) and the deformation of the copper cluster ( $\Delta E_{\text{defCu}_n}$ ). Due to technical reasons, in the ADF program, this energy decomposition analysis can be performed only on singlet state fragments. For this reason in clusters having an odd number of copper atoms, it is necessary to correct the interaction energy by adding an energy term, the so-called excitation energy, that accounts for the energy difference between the fictitious singlet state (with half  $\alpha$  and  $\beta$  electrons in the HOMO) taken as the reference in the EDA analysis and the real doublet state.<sup>48</sup>

Table 3 collects the results of the EDA. For the different copper cluster carbonyls, the values of  $\Delta E_{\text{def}}$  do not exceed 1.4 kcal·mol<sup>-1</sup>, except for Cu<sub>5</sub>CO and Cu<sub>6</sub>CO due to the important geometrical changes undergone by the bare cluster geometry with the adsorption of CO. The deformation of the CO molecule is always small, ranging between 0.1 and 0.5 kcal·mol<sup>-1</sup>. The  $\Delta E_{\text{excit}}$  term decreases with the size of the cluster. Thus, the energy difference between the fictitious singlet state and the doublet state in Cu<sub>1</sub> is 4.4 kcal·mol<sup>-1</sup> higher than that of the Cu<sub>9</sub> bare cluster. Extrapolation of this result points out that the  $\Delta E_{\text{excit}}$  term will be close to zero for bigger clusters, and null for the copper surface. Like the  $\Delta E_{\text{excit}}$  term, in general,  $\Delta E_{\text{prep}}$  decreases upon the size of the cluster, indicating that in the limit of the metallic bulk this term will likely become insignificant. The  $\Delta E_{\text{int}}$  ranges between 22 and 44 kcal·mol<sup>-1</sup>. This term is useful to describe the different behavior of the clusters with respect to the interaction with CO. The interaction energy term can be also divided into Pauli repulsion ( $\Delta E_{\text{Pauli}}$ ), electrostatic interaction ( $\Delta E_{\text{elstat}}$ ), and orbital interaction ( $\Delta E_{\text{oi}}$ ). There is a relationship between the Cu–C bond and the different components of the interaction energy. In general, the longer the Cu–C bond length, the smaller (in absolute values) are the  $\Delta E_{\text{int}}$ ,  $\Delta E_{\text{Pauli}}$ ,  $\Delta E_{\text{elstat}}$ , and  $\Delta E_{\text{oi}}$  terms. The correlation between the Cu–C bond distances and the  $\Delta E_{\text{int}}$  term presents a regression coefficient ( $r^2$ ) of 0.820. Moreover, if we leave out the value of the Cu<sub>1</sub>CO species, the  $r^2$  value improves to 0.882. This exclusion is often carried out in the bibliography.<sup>26,29,32</sup> The energy  $\Delta E_{\text{oi}}$  presents a good correlation with the Cu–C and the C–O bond lengths. In this latter case,  $r^2$  is 0.860 if the value of the Cu<sub>3</sub>CO cluster is left out.

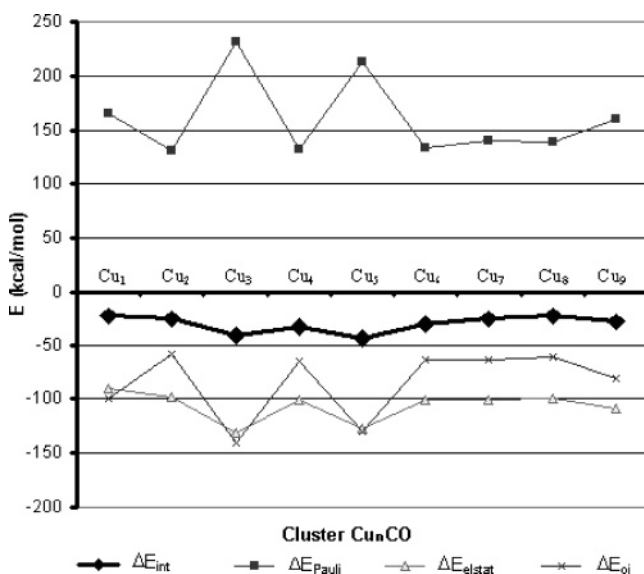
Figure 6 plots the values of  $\Delta E_{\text{int}}$  and of its three components for the most stable copper cluster carbonyls. It is worth noting that the values of the components of the interaction energy as well as the total interaction energy present an oscillating behavior that apparently converges for the largest clusters. As can be seen in this Figure, the behavior of the  $\Delta E_{\text{int}}$  parallels that of the  $\Delta E_{\text{oi}}$  and  $\Delta E_{\text{elstat}}$  terms, while the  $\Delta E_{\text{Pauli}}$  follows an opposite trend. Indeed, the correlation between the  $\Delta E_{\text{Pauli}}$  and  $\Delta E_{\text{oi}}$  terms is quite large ( $r^2 = 0.945$ ). Better orbital interactions ( $\Delta E_{\text{oi}}$ ) lead to smaller Cu–C bonds and larger absolute values  $\Delta E_{\text{elstat}}$  and  $\Delta E_{\text{Pauli}}$  interactions. This is particularly true for the Cu<sub>3</sub>CO and Cu<sub>5</sub>CO species. The percentage of ionic character

**TABLE 4:  $\Delta E_{\text{oi}}$  Decomposition for Cu<sub>n</sub>CO ( $n = 1-8$ ) (energies given in kcal·mol<sup>-1</sup>)**

cluster	$\Delta E_{\text{oi}}$	$\Delta E_{\sigma}$	$\Delta E_{\pi}$	% $\sigma$	% $\pi$
Cu <sub>1</sub> CO	-98.8	-88.3	-10.5	89.4	10.6
Cu <sub>2</sub> CO	-58.3	-42.4	-15.9	72.8	27.2
Cu <sub>3</sub> CO	-140.1	-126.1	-14.0	90.0	10.0
Cu <sub>4</sub> CO	-64.7	-43.3	-21.4	66.9	33.1
Cu <sub>5</sub> CO	-129.4	-110.9	-18.5	85.7	14.3
Cu <sub>6</sub> CO	-64.0	-47.1	-16.9	73.6	26.4
Cu <sub>7</sub> CO	-64.2	-45.6	-18.6	71.1	28.9
Cu <sub>8</sub> CO	-61.2	-46.2	-15.0	75.5	24.5

of the CO interaction in the copper cluster carbonyls ranges between 50 and 60%, approximately. It is smaller for open-shell clusters with an odd number of copper atoms than for closed-shell clusters due to the fact that the former present better orbital interactions because of the presence of a semioccupied molecular orbital (SOMO) that can participate in the bonding as a high-lying HOMO or low-lying LUMO.

To analyze further the orbital interaction energy term, we have taken advantage of the symmetry plane of the Cu<sub>n</sub>CO clusters from  $n = 1$  to 8 to separate the  $\sigma$  and  $\pi$  orbital interaction energy parts. From the results in Table 4, we can see that, first, the donation ( $\Delta E_{\sigma}$ ) linked to the HOMO of CO and LUMO of Cu<sub>n</sub> interaction in the DCD bonding scheme (vide supra) is more than twice as large as the term associated with back-donation ( $\Delta E_{\pi}$ ), and, second, there is not a clear-cut relationship between the  $\Delta E_{\sigma}$  and  $\Delta E_{\pi}$  values. Thus, higher  $\Delta E_{\sigma}$  energies do not imply also larger  $\Delta E_{\pi}$  values. In fact, a higher value of  $\Delta E_{\text{oi}}$  is reflected only in  $\Delta E_{\sigma}$  ( $r^2 = 0.992$ ). Finally, back-donation is especially high in the smallest clusters with

**Figure 6.** Interaction energy of the Cu<sub>n</sub>CO clusters and its components. Energies are given in kcal·mol<sup>-1</sup>.



**TABLE 5: Mayer Bond Orders for the Most Stable  $\text{Cu}_n\text{CO}$  ( $n = 1-9$ )**

cluster	Cu–C	C–O
$\text{Cu}_1\text{CO}$	1.02	2.11
$\text{Cu}_2\text{CO}$	0.87	2.18
$\text{Cu}_3\text{CO}$	0.91	2.13
$\text{Cu}_4\text{CO}$	0.88	2.15
$\text{Cu}_5\text{CO}$	0.92	2.13
$\text{Cu}_6\text{CO}$	0.89	2.15
$\text{Cu}_7\text{CO}$	0.88	2.16
$\text{Cu}_8\text{CO}$	0.87	2.17
$\text{Cu}_9\text{CO}$	0.88	2.14

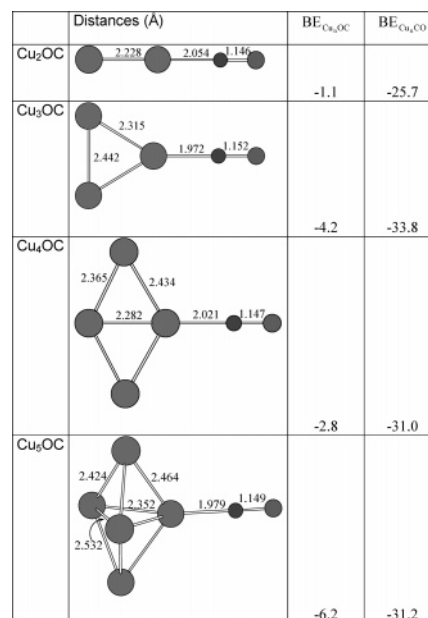
**TABLE 6: CO Hirshfeld Charges in  $\text{Cu}_n\text{CO}$  and Reduction of the CO HOMO Mulliken Charge (donation) and Increase of the CO LUMO and LUMO+1 Mulliken Charge (back-donation) in the  $\text{Cu}_n\text{CO}$  Clusters (charges in electrons)**

cluster	CO charge	donation	back-donation
$\text{Cu}_1\text{CO}$	-0.079	0.29	0.40
$\text{Cu}_2\text{CO}$	0.013	0.29	0.26
$\text{Cu}_3\text{CO}$	-0.046	0.33	0.38
$\text{Cu}_4\text{CO}$	-0.037	0.33	0.35
$\text{Cu}_5\text{CO}$	-0.048	0.36	0.38
$\text{Cu}_6\text{CO}$	-0.042	0.36	0.34
$\text{Cu}_7\text{CO}$	-0.032	0.33	0.33
$\text{Cu}_8\text{CO}$	-0.020	0.33	0.31
$\text{Cu}_9\text{CO}$	-0.054	0.35	0.36

an odd number of copper atoms. We note in passing that the fact that donation is more important than back-donation was also found for the interaction of carbene in Fischer carbene complexes.<sup>72</sup>

The Mayer bond orders (MBOs) for the most stable  $\text{Cu}_n\text{CO}$  structures are listed in Table 5. The MBO values for  $\text{Cu}_1\text{CO}$  reflect the particular behavior of this copper cluster carbonyl as compared to the other clusters. The MBOs point out that  $\text{Cu}_1\text{CO}$  has the strongest Cu–C bond and the weakest C–O bond. In general, the odd-numbered copper clusters have higher Cu–C and lower C–O MBOs when compared to the even-numbered ones. This is in line with the better orbital interactions found in the EDA analysis for the copper clusters with an odd number of copper atoms. The C–O MBO value for the free CO molecule is 2.28. Therefore, the C–O is clearly activated in copper cluster carbonyls as the MBO decreases when the CO is coordinated to a copper cluster. When the size of the cluster increases, the oscillator behavior of the Cu–C and C–O MBOs tends to disappear.

Table 6 collects the Hirshfeld charge values of the CO fragment in the copper cluster carbonyls. The charge values close to zero for the CO fragment show that, from the Hirshfeld charge analysis viewpoint, the  $\text{Cu}_n$  back-donation of charge to CO is as important as the donation of CO toward the copper cluster. Although one might expect a larger charge donation than back-donation according to the EDA analysis, the Mulliken charge lost by the HOMO of CO (about 0.3–0.4 au) and the Mulliken charge acquired by the LUMO and LUMO+1 of CO (0.3–0.4 au) in the metal cluster carbonyls supports the conclusion that donation and back-donation are equally important from a charge analysis point of view. Differences in the trends given by the EDA and charge analysis are not completely unexpected<sup>73</sup> because energetically not only the attractive interactions between orbitals are important but also the repulsive ones (from the charge point of view only the favorable orbital interactions contribute to the charge transfer). The elongation of the C–O bond distance is correlated with the LUMO and LUMO+1 occupations of the CO fragment in the copper cluster monocarbonyls ( $r^2 = 0.814$ ).

**Figure 7.** Molecular geometries and binding energies for the  $\text{Cu}_n\text{OC}$  clusters (energies in  $\text{kcal}\cdot\text{mol}^{-1}$ ).

**3. Binding of CO through the Oxygen Atom.** According to our calculations, the coordination of the CO molecule to the copper clusters through the oxygen atom is possible only for the copper clusters with  $n = 2-5$ . The molecular structure of these clusters together with their CO BE is given in Figure 7. The Cu–O bond distances are about 2 Å for all optimized  $\text{Cu}_n\text{OC}$  clusters, somewhat larger than the Cu–C bond lengths of the  $\text{Cu}_n\text{CO}$  clusters. The CO binding through the oxygen atom involves binding energies that are about 25–30  $\text{kcal}\cdot\text{mol}^{-1}$  lower in absolute value than those that come from the interaction through the carbon atom. The BE difference between the CO binding through the carbon as compared to through the oxygen atom increases with the size of the cluster. Indeed, for the higher members of the series, the binding of CO is an endothermic process and the geometry optimization of the initial  $\text{Cu}_n\text{OC}$  clusters leads to the  $\text{Cu}_n$  and CO separated fragments. Extrapolating this result to a copper surface, we conclude that coordination of CO through the oxygen atom is not possible. In fact, the Mulliken condensed Fukui function analysis of the CO molecule gives values of 0.759 and 0.241 for the  $f^-$  function of the carbon and the oxygen atoms, respectively, and of 0.866 and 0.134 for the  $f^+$  function. Therefore, an electrophilic or nucleophilic attack through the oxygen atom of CO is not favored according to the condensed Fukui values.

## 5. Conclusions

This study has analyzed the adsorption of CO on small copper clusters,  $\text{Cu}_n$  ( $n = 1-9$ ). It has been confirmed that the bare copper clusters with even number of copper atoms are more stable than those with an odd number of copper atoms. The latter are the most reactive and, in fact, they show the higher CO binding energies. We have found that the nucleophilic condensed Fukui function and the shape of the LUMO orbitals are useful tools to predict the regioselectivity of the CO insertion, with the only exception being the  $\text{Cu}_7$  cluster. The energy decomposition analyses of the CO binding energy in the copper cluster carbonyls have shown that the  $\sigma$  donation is about twice as important as  $\pi$  back-donation. From an electron charge point of view, however, donation and back-donation are equally important. Finally, we have shown that the coordination

of CO through the oxygen is energetically unfavorable as compared to CO binding through the carbon atom, especially for the larger copper clusters.

**Acknowledgment.** This work is dedicated in memory of our friend Dr. Xavier Gironès “Giro”, who died on 27 November 2005. This research has been financed by MEC of Spain through the projects CTQ2005-08797-C02-01, BQU2002-03334, and BQU2002-04112-C02-02, and by FONDECYT of Chile through the project 1020534. We are grateful to the referees for helpful comments. P.J. is grateful to MECESUP (PUC-0004, Red Química UCH-0116) for a postdoctoral fellowship. M.S. is indebted to the Departament d’Universitats, Recerca i Societat de la Informació (DURSI) of the Generalitat de Catalunya for financial support through the Distinguished University Research Promotion, 2001. A.P. is grateful for the award of a doctoral grant from MEC and for the helpful comments given by E. Matito, M. Torrent, P. Salvador, and Ll. Blancafort. We thank the Centre de Supercomputació de Catalunya (CESCA) for partial funding of computer time.

**Supporting Information Available:** Results from other less stable structures of neutral  $\text{Cu}_n$  ( $n = 2-9$ ) clusters, including frequencies of the copper clusters and XYZ coordinates of the most stable BPW91 optimized  $\text{Cu}_n$  and  $\text{Cu}_n\text{CO}$  complexes. This material is available free of charge via the Internet at <http://pubs.acs.org>.

## References and Notes

- Morse, M. D. *Chem. Rev.* **1986**, *86*, 1049–1109.
- Zacarias, A. G.; Castro, M.; Tour, J. M.; Seminario, J. M. *J. Phys. Chem. A* **1999**, *103*, 7692–7700.
- Seminario, J. M.; Tour, J. M. *Int. J. Quantum Chem.* **1997**, *65*, 749–758.
- Mineva, T.; Russo, N.; Toscano, M. *Int. J. Quantum Chem.* **2000**, *80*, 105–109.
- Jaques, P.; Toro-Labbé, A. *J. Phys. Chem. B* **2004**, *108*, 2568–2574.
- Koretsky, G. M.; Knickelbein, M. B. *J. Chem. Phys.* **1997**, *106*, 9810–9814. (b) Knight, W. D.; Clemenger, K.; de Heer, W. A.; Saunders, W. A. *Phys. Rev. Lett.* **1984**, *52*, 2141–2143. (c) Kreibeg, V.; Vollmer, M. *Optical Properties of Metal Clusters*; Springer: Berlin, 1995. (d) Zhao, Y.; Xu, W.; Li, W.; Xie, Y.; Schaefer, H. F., III *J. Comput. Chem.* **2004**, *25*, 907–920. (e) Chandrakumar, K. R. S.; Ghanty, T. K.; Ghosh, S. K. *J. Phys. Chem. A* **2004**, *108*, 6661–6666. (f) Fournier, R. *J. Chem. Phys.* **2001**, *115*, 2165–2177.
- Knickelbein, M. B. *Chem. Phys. Lett.* **1992**, *192*, 129–134.
- Powers, D. E.; Hansen, S. G.; Geusic, M. E.; Michalopoulos, D. L.; Smalley, R. E. *J. Chem. Phys.* **1983**, *78*, 2866–2881.
- Spasov, V. A.; Lee, T.-H.; Ervin, K. M. *J. Chem. Phys.* **2000**, *112*, 1713–1720.
- Ingólfsson, O.; Busolt, U.; Sugawara, K. *J. Chem. Phys.* **2000**, *112*, 4613–4620.
- Holmgren, L.; Gronbeck, H.; Andersson, M.; Rosen, A. *Phys. Rev. B* **1996**, *53*, 16644–16651.
- Winter, B. J.; Parks, E. K.; Riley, S. J. *J. Chem. Phys.* **1991**, *94*, 8618–8621.
- Lammers, V.; Borstel, G. *Phys. Rev. B* **1994**, *49*, 17360–17377.
- Fuentealba, P.; Simón-Manso, Y. *Chem. Phys. Lett.* **1999**, *314*, 108–113.
- Ho, J.; Ervin, K. M.; Lineberger, W. C. *J. Chem. Phys.* **1990**, *93*, 6987–7002.
- Aakeby, H.; Panas, I.; Pettersson, L. G. M.; Siegbahn, P. E. M.; Wahlgren, U. *J. Phys. Chem.* **1990**, *94*, 5471–5477.
- Balbuena, P.; Derosa, P.; Seminario, J. M. *J. Phys. Chem. B* **1999**, *103*, 2830–2840.
- Padilla-Campos, L.; Toro-Labbé, A.; Maruani, J. *Surf. Sci.* **1997**, *384*, 24–36.
- Padilla-Campos, L.; Toro-Labbé, A. *J. Mol. Struct. (THEOCHEM)* **1997**, *390*, 183–192.
- Padilla-Campos, L.; Toro-Labbé, A. *J. Chem. Phys.* **1998**, *108*, 6458–6465.
- Calaminici, P.; Köster, A. M.; Russo, N.; Salahub, D. R. *J. Chem. Phys.* **1996**, *105*, 9546–9556.
- Calaminici, P.; Jug, K.; Köster, A. M. *J. Chem. Phys.* **1998**, *109*, 7756–7763.
- Calaminici, P.; Köster, A. M.; Vela, A. *J. Chem. Phys.* **2002**, *113*, 2199–2202. (b) Yang, M.; Jackson, K. A. *J. Chem. Phys.* **2005**, *122*, 184317.
- Mossobrio, C.; Pasquarello, A.; Dal Corso, A. *J. Chem. Phys.* **1998**, *109*, 6626–6630.
- Jackson, K. A. *Phys. Rev. B* **1993**, *47*, 9715–9722.
- Jug, K.; Zimmermann, B.; Calaminici, P.; Köster, A. M. *J. Chem. Phys.* **2002**, *116*, 4497–4507.
- Huber, K. P.; Herzberg, G. *Molecular Spectra and Molecular Structure*; Van Nostrand-Reinhold: New York, 1989; Vol. IV.
- Rohlfing, E. A.; Valentini, J. J. *J. Chem. Phys.* **1986**, *84*, 6560–6566.
- Jaques, P.; Toro-Labbé, A. *J. Chem. Phys.* **2002**, *117*, 3208–3218.
- Crispin, X.; Bureau, C.; Geskin, V.; Lazzaroni, R.; Brédas, J.-L. *Eur. J. Inorg. Chem.* **1999**, 349–360.
- Schmid, G. *Chem. Rev.* **1992**, *92*, 1709–1727.
- Cao, Z.; Wang, Y.; Zhu, J.; Wu, W.; Zhang, Q. *J. Phys. Chem. B* **2002**, *106*, 9649–9654.
- Nygren, M. A.; Siegbahn, P. E. M. *J. Phys. Chem.* **1992**, *96*, 7579–7584. (b) Nygren, M. A.; Siegbahn, P. E. M.; Jin, C.; Guo, T.; Smalley, R. E. *J. Chem. Phys.* **1991**, *95*, 6181–6184.
- Taylor, K. J.; Pettiette-Hall, C. L.; Cheshnovsky, O.; Smalley, R. E. *J. Chem. Phys.* **1992**, *96*, 3319–3329.
- Wheeler, S. E.; Sattelmeyer, K. W.; Scheleyer, P. v. R.; Schaefer, H. F., III *J. Chem. Phys.* **2004**, *120*, 4683–4689.
- Chattaraj, P. K.; Fuentealba, P.; Jaques, P.; Toro-Labbé, A. *J. Phys. Chem. A* **1999**, *103*, 9307–9312.
- Gutiérrez-Oliva, S.; Jaques, P.; Toro-Labbé, A. *J. Phys. Chem. A* **2000**, *104*, 8955–8964.
- Toro-Labbé, A. *J. Phys. Chem. A* **1999**, *103*, 4398–4403.
- Jaques, P.; Toro-Labbé, A. *J. Phys. Chem. A* **2000**, *104*, 995–1003.
- Parr, R. G.; Yang, W. *J. Am. Chem. Soc.* **1984**, *106*, 4049–4050.
- Kohn, W.; Becke, A. D.; Parr, R. G. *J. Phys. Chem.* **1996**, *100*, 12974–12980.
- Perdew, J. P.; Parr, R. G.; Levy, M.; Balduz, J. L. *Phys. Rev. Lett.* **1982**, *49*, 1691–1694.
- Yang, W.; Parr, R. G.; Pucci, R. *J. Chem. Phys.* **1984**, *81*, 2862–2863.
- Yang, W.; Mortier, W. J. *J. Am. Chem. Soc.* **1986**, *108*, 5708–5711.
- Bickelhaupt, F. M.; Nibbering, N. M.; van Wezenbeek, E. M.; Baerends, E. J. *J. Phys. Chem.* **1992**, *96*, 4864–4873. (b) Ziegler, T.; Rauk, A. *Inorg. Chem.* **1979**, *18*, 1558–1565. (c) Ziegler, T.; Rauk, A. *Inorg. Chem.* **1979**, *18*, 1755–1759. (d) Ziegler, T.; Rauk, A. *Theor. Chim. Acta* **1977**, *46*, 1–10. (e) Kitaura, K.; Morokuma, K. *Int. J. Quantum Chem.* **1976**, *10*, 325–331.
- Lein, M.; Szabó, A.; Kovács, A.; Frenking, G. *Faraday Discuss.* **2003**, *124*, 365–378.
- Mayer, I. *Chem. Phys. Lett.* **1983**, *97*, 270–274. (b) Mayer, I. *Int. J. Quantum Chem.* **1984**, *26*, 151–154. (c) Mayer, I. *Int. J. Quantum Chem.* **1986**, *29*, 73–84. (d) Mayer, I. *Int. J. Quantum Chem.* **1986**, *29*, 477–483.
- González-Blanco, O.; Branchadell, V.; Monteyne, K.; Ziegler, T. *Inorg. Chem.* **1998**, *37*, 1744–1748.
- ADF2002.03. Baerends, E. J.; Autschbach, J. A.; Bérces, A.; Bo, C.; Boerrigter, P. M.; Cavallo, L.; Chong, D. P.; Deng, L.; Dickson, R. M.; Ellis, D. E.; Fan, L.; Fischer, T. H.; Fonseca Guerra, C.; van Gisbergen, S. J. A.; Groeneveld, J. A.; Gritsenko, O. V.; Grüning, M.; Harris, F. E.; van den Hoek, P.; Jacobsen, H.; van Kessel, G.; Kootstra, F.; van Lenthe, E.; Osinga, V. P.; Patchkovskii, S.; Philippen, P. H. T.; Post, D.; Pye, C. C.; Ravenek, W.; Ros, P.; Schipper, P. R. T.; Schreckenbach, G.; Snijders, J. G.; Solà, M.; Swart, M.; Swerhone, D.; te Velde, G.; Vermooijs, P.; Versluis, L.; Visser, O.; van Wezenbeek, E.; Wiesenekker, G.; Wolff, S. K.; Woo, T. K.; Ziegler, T. *Vrije Universiteit Amsterdam*: Amsterdam, The Netherlands, 2002.
- Baerends, E. J.; Ellis, D. E.; Ros, P. *Chem. Phys.* **1973**, *2*, 41–51.
- Fonseca Guerra, C.; Visser, O.; Snijders, J. G.; te Velde, G.; Baerends, E. J. *Methods and Techniques for Computational Chemistry*; STEF: Cagliari, 1995; p 305.
- te Velde, G.; Bickelhaupt, F. M.; Baerends, E. J.; Fonseca Guerra, C.; van Gisbergen, S. J. A.; Snijders, J. G.; Ziegler, T. *J. Comput. Chem.* **2001**, *22*, 931–967.
- te Velde, G.; Baerends, E. J. *J. Comput. Phys.* **1992**, *99*, 84–98.
- Becke, A. D. *Phys. Rev. A* **1988**, *38*, 3098–3100. (b) Becke, A. D. *J. Chem. Phys.* **1986**, *84*, 4524–4529. (c) Becke, A. D. *Int. J. Quantum Chem.* **1983**, *23*, 1915–1922.
- Perdew, J. P. *Phys. Rev. B* **1986**, *33*, 8822–8824. (b) Perdew, J. P.; Wang, W. R. *Phys. Rev. B* **1992**, *45*, 13244–13249.

- (56) Versluis, L.; Ziegler, T. *J. Chem. Phys.* **1988**, *88*, 322. (b) Fan, L.; Ziegler, T. *J. Chem. Phys.* **1991**, *95*, 7401–7408. (c) Schreckenbach, G.; Li, J.; Ziegler, T. *Int. J. Quantum Chem.* **1995**, *56*, 477–488.
- (57) Fan, L.; Versluis, L.; Ziegler, T.; Baerends, E. J.; Ravenek, W. *Int. J. Quantum Chem. Symp.* **1988**, *22*, 173–181.
- (58) Jacobsen, H.; Schreckenbach, G.; Ziegler, T. *J. Phys. Chem.* **1994**, *98*, 11406–11410.
- (59) Snijders, J. G.; Baerends, E. J.; Vernooijs, P. *At. Nucl. Data Tables* **1982**, *26*, 483–509.
- (60) Vernooijs, P.; Baerends, E. J. *Slater Type Basis Functions for the Whole Periodic System. Internal Report 1*; Vrije Universiteit of Amsterdam, The Netherlands, 1981.
- (61) Krijn, J.; Baerends, E. J. *Fit Functions in the HFS Method. Internal Report (in Dutch)*; Vrije Universiteit of Amsterdam, The Netherlands, 1984.
- (62) MOLEKEL 4.0, Flükiger, P.; Lüthi, H. P.; Portmann, S.; Weber, J. Swiss Center for Scientific Computing; Manno (Switzerland), 2000.
- (63) Florez, E.; Tiznado, W.; Mondragón, F.; Fuentealba, P. *J. Phys. Chem. A* **2005**, *109*, 7815–7821.
- (64) Massobrio, C.; Pasquarello, A.; Dal Corso, A. *J. Chem. Phys.* **1998**, *109*, 6626–6630.
- (65) Elschenbroich, Ch.; Salzer, A. In *Organometallics: A Concise Introduction*, 2nd ed.; VCH: Weinheim, Germany, 1992.
- (66) Dewar, M. J. S. *Bull. Soc. Chim. Fr.* **1951**, *18*, C71–9. (b) Chatt, J.; Duncanson, L. A. *J. Chem. Soc.* **1953**, 2939–2947.
- (67) Arulmozhiraja, S.; Kolandaivel, P. *Mol. Phys.* **1997**, *90*, 55–62. (b) Fuentealba, P.; Pérez, P.; Contreras, R. *J. Chem. Phys.* **2000**, *113*, 2544–2551. (c) Roy, R. K.; Hirao, K. *J. Chem. Phys.* **2001**, *115*, 2901–2907. (d) De Profit, F.; Van Alsenoy, C.; Peeters, A.; Langenaeker, W.; Geerlings, P. *J. Comput. Chem.* **2002**, *23*, 1198–1209. (e) Roy, R. K.; Pal, S.; Hirao, K. *J. Chem. Phys.* **1999**, *110*, 8236–8245.
- (68) Fonseca Guerra, C.; Handgraaf, J.-W.; Baerends, E. J.; Bickelhaupt, F. M. *J. Comput. Chem.* **2004**, *25*, 189–210.
- (69) Chattaraj, P. K.; Lee, H.; Parr, R. G. *J. Am. Chem. Soc.* **1991**, *113*, 1855–1856. (b) Li, Y.; Evans, J. N. S. *J. Am. Chem. Soc.* **1995**, *117*, 7756–7759. (c) Parr, R. G.; Pearson, R. G. *J. Am. Chem. Soc.* **1983**, *105*, 7512–7516.
- (70) Ghosh, S. K.; Berkowitz, M. *J. Chem. Phys.* **1985**, *83*, 2976–2983. (b) Berkowitz, M.; Ghosh, S. K.; Parr, R. G. *J. Am. Chem. Soc.* **1985**, *107*, 6811–6814. (c) Berkowitz, M.; Parr, R. G. *J. Chem. Phys.* **1988**, *88*, 2554–2557.
- (71) Jug, K.; Zimmermann, B.; Köster, A. M. *Int. J. Quantum Chem.* **2002**, *90*, 594–602.
- (72) Vyboishchikov, S. F.; Frenking, G. *Chem. Eur. J.* **1998**, *4*, 1428–1438. (b) Cases, M.; Frenking, G.; Duran, M.; Solà, M. *Organometallics* **2002**, *21*, 4182–4191.
- (73) Frenking, G.; Solà, M.; Vyboishchikov, S. F. *J. Organometallic Chem.* **2005**, *690*, 6178–6204.